Experimental Response of Buildings Designed with Metallic Structural Fuses. II

Ramiro Vargas[1] and Michel Bruneau[2]

Abstract: In a companion paper, an alternative design approach was proposed to concentrate damage on disposable and easy to repair structural elements (i.e., "structural fuses"), while the main structure is designed to remain elastic or with minor inelastic deformations. To verify and validate the developed design procedure, an experimental project was conducted on the shaking table at the University at Buffalo, which consists of a three-story frame designed with buckling-restrained braces (BRBs) working as metallic structural fuses. This experimental project also assesses the replaceability of BRBs designed as sacrificeable and easy-to-repair members. These BRBs are connected to the frame by removable and eccentric gusset plate, especially designed to prevent performance problems observed in other experimental research. Design and behavior of this type of connection is also investigated here. Another objective of this test is to examine the use of seismic isolation devices to protect nonstructural components from severe floor vibrations in buildings designed per the structural fuse concept. The seismic isolation device consists of a bearing with a spherical ball rolling in conical steel plates, also called a ball-in-cone system. This type of seismic isolator was installed on the top floor of the frame model, and its response in terms of acceleration and displacement is investigated as part of this investigation.

DOI: 10.1061/(ASCE)0733-9445(2009)135:4(394)

CE Database subject headings: Structural design; Steel structures; Seismic design; Seismic effects; Damping; Inelasticity; Ductility; Shake table tests.

Introduction

Passive energy dissipation (PED) devices have been implemented in recent years to enhance structural performance by reducing seismically induced structural damage (and, indirectly to some extent, nonstructural damage). Soong and Spencer (2002) reported that, in the last 16 years, more than 100 buildings in North America have been either retrofitted or built using PED devices. In the meantime, Japan has employed these structural protective systems in hundreds of buildings.

PED metallic dampers (or hysteretic dampers) dissipate energy via inelastic deformations. Since their response is not sensitive to the frequency of loading, they are also called rate-independent dampers, or displacement-dependent dampers. The amount of damping they provide is somewhat proportional to the magnitude of their inelastic deformations. Although they also increase the stiffness of the primary structure to some degree, the possible increase in input energy due to the added stiffness is dissipated as part of the total hysteretic behavior of properly designed dampers, resulting in a net reduction on the response of the structural system in terms of lateral displacements, compared to response of the system without dampers. Accelerations and lateral forces are either increased or reduced depending on the ground motion and system features. Metallic dampers are defined here to be structural fuses when they are designed such that all damage is concentrated on the PED devices, allowing the primary structure to remain elastic.

In a companion paper, a procedure to design and retrofit structural fuse systems was presented, based on a parametric analysis conducted for single-degree-of-freedom (SDOF) systems. As a proof of concept to the developed design procedure, this paper describes an experimental testing on the shaking table at University of Buffalo of a three-story frame designed with buckling-restrained braces (BRBs) acting as metallic structural fuses. This experimental project also assesses the replaceability of BRBs designed as sacrificeable and easy- to-repair elements. Eccentric gusset plate, especially designed to prevent performance problems observed in previous experimental research (e.g., local instability of concentric gusset plates as reported by Tsai et al. 2004; Mahin et al. 2004; Uriz 2005) are used for the connection of BRBs. As part of this test, a seismic isolation device is installed on the experimental frame to examine its effectiveness in the protection of nonstructural components from severe floor vibrations, as a conscious attempt to provide an integral performance-based approach to the building and nonstructural systems. Furthermore, a series of uniaxial static tests were conducted to experimentally determine the cyclic characteristics of the BRBs, and comparisons between results obtained from static and dynamic tests are also discussed.

[1]Assistant Professor, Dept. of Civil Engineering, Technological Univ. of Panama, PTY #12450, P.O. Box 25207, Miami, FL 33102 (corresponding author). E-mail: ramiro.vargas@utp.ac.pa

[2]Professor and MCEER Director, Dept. of Civil, Structural and Environmental Engineering, State Univ. of New York at Buffalo, 130 Ketter Hall, Buffalo, NY 14260. E-mail: bruneau@buffalo.edu

Note. Associate Editor: Marvin W. Halling. Discussion open until September 1, 2009. Separate discussions must be submitted for individual papers. The manuscript for this paper was submitted for review and possible publication on August 31, 2007; approved on September 5, 2008. This paper is part of the ***Journal of Structural Engineering***, Vol. 135, No. 4, April 1, 2009. ©ASCE, ISSN 0733-9445/2009/4-394–403/$25.00.

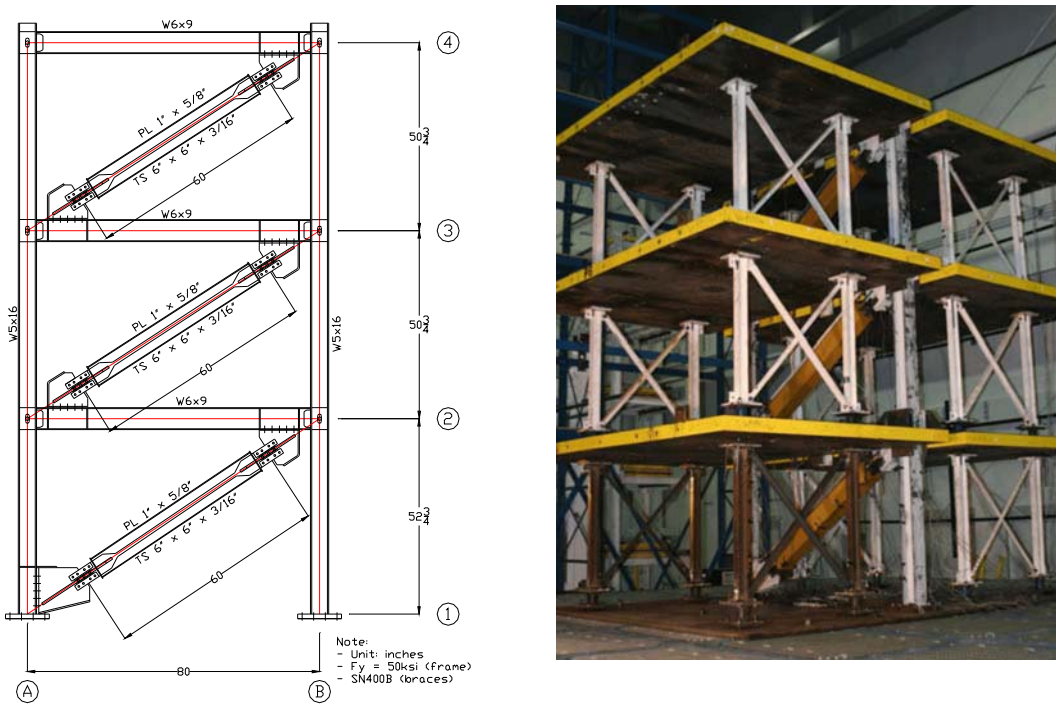

Fig. 1. Experiment setup: (a) frame with Nippon steel BRBs; (b) general view of experiment

Frame and BRBs Description

General

The three-story one-bay frame specimen tested is a model of the design example from the companion paper taken as a prototype. Frame members were designed using steel with a yield stress of 345 MPa (50 ksi). The model is a two-dimensional structure designed with BRBs manufactured by Nippon Steel Corporation, as shown in Fig. 1(a). Note that the bare frame (BF) was designed to be used in repeatable tests with two sets of BRBs. A general view of the experiment setup can be seen in Fig. 1(b).

BRB cores consist of a rectangular plate (16 mm × 25 mm) made of SN400B steel (F_y=235 MPa, and F_u=400 MPa), which expands at the ends to form a cruciform section. A steel tube (HSS 6×6×3/16) filled with mortar surrounds the core to prevent buckling of the plate and ensure a similar behavior in tension and compression of the brace.

Scaling

Due to loading equipment constraints, specimen components and mass were scaled using a scale factor of 1/3 for geometric quantities and 1/18 for the mass (i.e., S_L=1/3, and S_M=1/18). Since the gravity loads for the model were carried by an independent gravity columns system (described later), the acceleration scale factor, S_A, can be established different from one, according to the following similitude relation: $S_A=S_L^2/S_M=(1/3)^2/(1/18)=2$. Accordingly, time-scale factor, S_T, was: $S_T=(S_L/S_A)^{1/2}=((1/3)/2)^{1/2}=0.4082$, which implies that the ground motion ordinates and time step were multiplied by 2 and 0.4082, respectively. The component properties of the model are shown in Table 1.

Target parameters for the prototype (i.e., α=0.25, μ_{max}=5, and η=0.25) can be applied directly to the model, since they are dimensionless quantities that are not affected by scale factors. However, the prototype period limit (i.e., $T \leqslant 1.80$ s) should be reduced by the corresponding time scaled factor (i.e., S_T=0.408) to obtain the period limit for the model (i.e., $T \leqslant 1.80 \cdot 0.408 = 0.73$ s). Actual parameters and elastic period are determined from pushover and eigenvalue analyses, respectively, and results are: α=0.12, μ_{max}=4.69, η=0.80, and T=0.22 s. Those values of α and μ_{max} are in fair agreement with the target parameters. However, some discrepancies may be noted between obtained and target values for η and T due to the incomplete similitude of the model. Despite these deviations from target parameters, it is noteworthy that actual parameters for the model system result in a behavior that still falls within the region of admissible solutions (according to the graphic representation in the first paper). Fig. 2 shows the pushover curves corresponding to the bare frame, BRBs, and the total base shear capacity of the system. Yield displacements of 7 and 34 mm for the BRBs and the bare frame, respectively, may be observed on this plot. In Fig. 2, it can also be noted that BRBs do not yield simultaneously, since all braces have identical properties, which is another consequence of the physical constraints in the model.

Gusset-Plates Description

To achieve the objective of facilitating the replaceability of BRBs designed to work as metallic structural fuses, gusset plates were

Table 1. Summary of Components for Model System

Story	Beams	Columns	BRB (mm)
3	W6×9	W5×16	PL 25×16
2	W6×9	W5×16	PL 25×16
1	W6×9	W5×16	PL 25×16

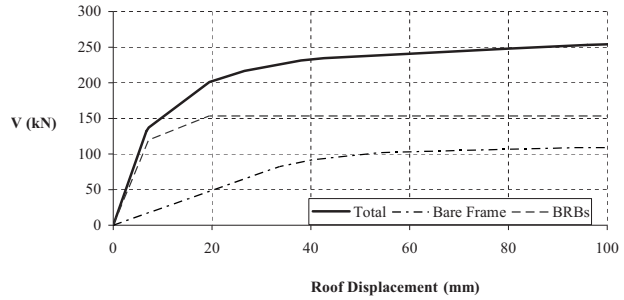

Fig. 2. Pushover curve for model

also designed as removable elements bolted to frame members. Typical gusset-plate details for the model are shown in Fig. 3. Note that the gusset plates are eccentrically connected only to beams with a separation of 76 mm (3 in.) from the columns. Although this is an eccentric connection, gusset plates were designed such that the center line of braces, beams, and columns coincide at the work point (i.e., intersection point between beams and column center lines).

These eccentric gusset plates were also used to prevent performance problems that have been observed in previous experimental studies of buckling-restrained braced frames with concentric connections (Tsai et al. 2004; Mahin et al. 2004; and Uriz 2005). Local buckling of gusset plates may occur when the angle between beam and column closes due to lateral displacements. In this experimental project, the 76 mm gap corresponds to half of the beam depth, and was selected to avoid any contact between gusset plates and columns during frame sway.

Rib stiffeners were also added to the gusset plates to improve local buckling capacity, as shown in Fig. 3, and the free edges of the gusset plates were restrained by lateral stiffeners to prevent out-of-plane buckling of the plates (Tsai et al. 2004).

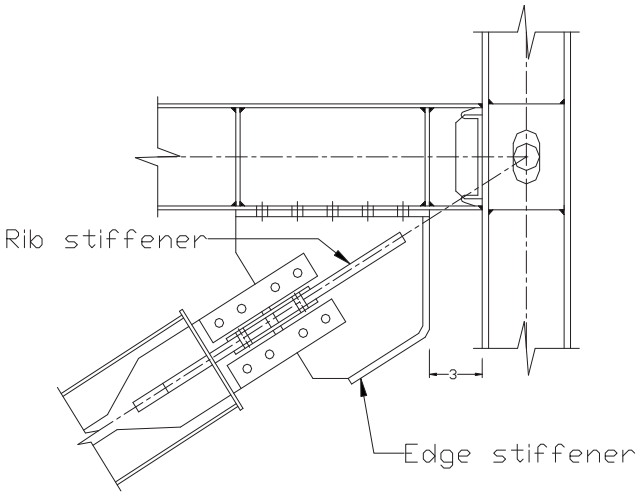

Fig. 3. Typical gusset-plate details

Seismic Isolation Device for Nonstructural Components

In Vargas and Bruneau (2006a) it was found that, in many cases, the use of metallic damper causes increases in floor accelerations, which may negatively affect the seismic behavior of nonstructural components. Since many nonstructural elements are vulnerable to shifting or overturning in structures designed or retrofitted with metallic dampers due to severe floor vibrations, the use of seismic isolation devices to protect them has been included in this experimental project. Seismic isolation is an extensively studied concept that has been widely implemented to protect structures from damaging earthquakes, by reducing seismic demands rather than strengthening the resistance capacity of structures (Naeim and Kelly 1999).

In this experimental study, the seismic isolation device used to protect nonstructural components consists of bearings with a spherical ball rolling in conical steel plates, as shown in Fig. 4. This rolling isolation system, also called a ball-in-cone (BNC) system, has been studied in the past as an alternative to decouple the dynamic response of structures from seismic ground motions (Kemeny and Szidarovszky 1995; Kasalanati et al. 1997; Amick et al. 1998 to name a few). The BNC isolator used in this study was manufactured and supplied by WorkSafe Technologies and called ISO-Base (U.S. Patent No. 5,599,106).

Fig. 4(a) shows the cross-section views of the bearing used in this study, which consists of four sets of steel plates interconnected by two plank assemblies. Conical plates have a diameter of 213 mm (8.375 in.). The slope of the cone is 1:10 (6°) with a maximum lateral displacement of 178 mm (7 in.). Conical plates are rounded at the apex with a radius of 127 mm (5 in.) to ensure a smooth response. Note that bearing thickness is only 76 mm (3 in.), which makes it attractive for floor isolation systems. From Fig. 4(b), it may be noted that the lateral displacement of the top plate is equal to twice the ball displacement.

Seismic response of the BNC bearing is a function of its geometric properties, which are schematically shown in Fig. 5(a) (greatly exaggerated here for clarity). Note that bearing plates have two distinct areas that govern the behavior: a spherical cen-

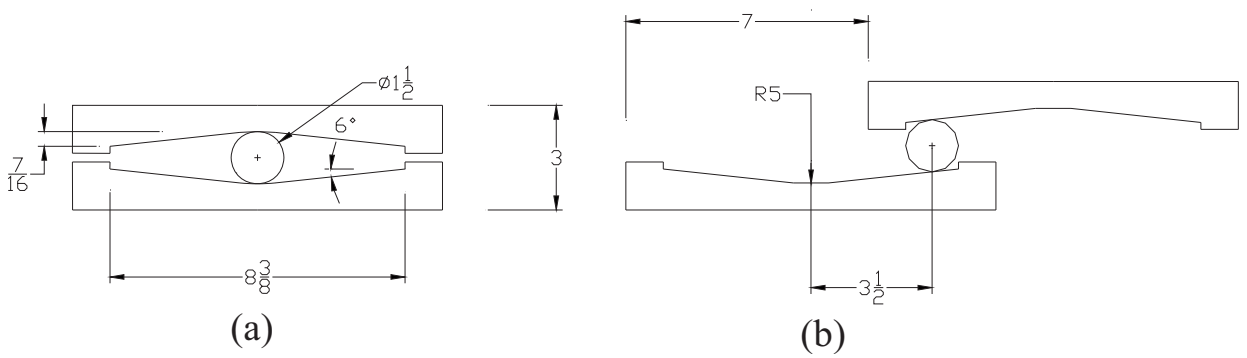

Fig. 4. Seismic isolation platform: (a) cross-sectional views of bearing; (b) bearing at maximum displacement

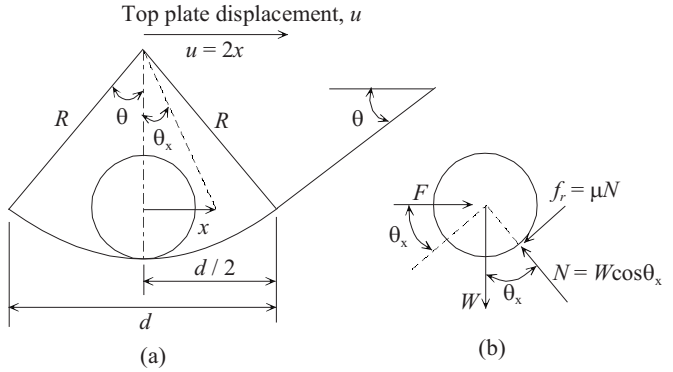

Fig. 5. Schematic representation of bearing geometry: (a) closeup of apex; (b) free-body diagram of rolling balls

tral area and a conical surface. From the free body diagram in Fig. 5(b), the governing equation of motion can be written as

$$F = \mu W \cos\theta_x + W\frac{x}{R\cos\theta_x} \tag{1}$$

where μ=friction coefficient between the balls and the plate surface; W=weight of the nonstructural component on top of the bearing; θ_x=rotational angle; and R=radius of the spherical central area; and x=balls lateral displacement. Since the rolling friction coefficient is very small (i.e., $\mu \approx 0$), and $\cos\theta_x \approx 1$, Eq. (1) can be simplified as

$$F = \frac{W}{R}x \tag{2}$$

which is valid when the ball is in the spherical central area ($x \leq d/2$). Knowing that the displacement of the top platform, u, is twice greater than the balls displacement (i.e., $u=2x$), Eq. (2) can be written in terms of the nonstructural component motion as

$$F = \frac{W}{2R}u \tag{3}$$

which is valid for $u \leq d$. When the balls reach the conical surface (i.e., $x > d/2$ or $u > d$), lateral force, F, is constant and independent of the lateral displacement (Kasalanati et al. 1997). In this conical area, Eq. (1) becomes

$$F = W\tan\theta\ \mathrm{sgn}(u) \approx W\theta\ \mathrm{sgn}(u) \tag{4}$$

where $\tan\theta$=cone slope, which is approximately equal to θ (in rad) for small angles.

Furthermore, in terms of acceleration demand, Eq. (4) can also be written as

$$a = g\tan\theta\ \mathrm{sgn}(u) \approx g\theta\ \mathrm{sgn}(u) \tag{5}$$

which in the case of bearings with a slope of 0.10, results in a constant acceleration response of 0.10 g. The force-displacement behavior of the BNC isolator can also be expressed as

$$F = \frac{F}{2R}u + \left(W\theta\ \mathrm{sgn}(u) - \frac{F}{2R}u\right)\cdot U(|u| - d) \tag{6}$$

where U=step function, which is equal to zero for $u < d$, and one for $u \geq d$.

Free vibration testing of the BNC isolator at hand showed maximum acceleration of 0.097 g [in good agreement with theoretical prediction from Eq. (5)], and a critical damping of 0.78% was calculated from logarithmic decay.

Since the rolling friction coefficient is negligible, the BNC isolator can be modeled as a multilinear elastic spring element, and its properties can be determined by Eqs. (3) and (4). Weight, W, was provided by lead bricks as 1.268 kN (0.285 kips), and from the isolator geometry the initial stiffness can be calculated as 0.0050 kN/mm (0.0285 kip/in.), with a spherical region, d, equal to 25.4 mm (1 in.). These properties were used in a SDOF model subjected to a base acceleration corresponding to the response of the third floor of the frame. A reduction of about 80% was observed in the peak acceleration response, along with a significant reduction in the frequency content of the response, due to the flexibility introduced by the isolator.

Gravity Columns System

The gravity columns system is a set of frames designed to separate the lateral resisting system from the vertical load resisting system, and has been used in various projects for structures near collapse at the University at Buffalo (Kusumastuti et al. 2005). These gravity frames consist of columns connected to rocking supports with the frame free to displace unrestrained in the longitudinal direction, and diagonally braced in the transverse direction. This set of gravity frames has been designed such that only vertical loads can be carried out by the columns.

Note that this gravity columns system is physically unable to support lateral loads. When the model is dynamically excited, lateral loads are transmitted to the testing frame by ϕ38 mm (1 1/2 in.) bolts. A machined hole was made at the midpoint of the column web at each beam level to match these pins. Doubler plates were used at both sides of the columns web to reinforce the panel zone, and the holes were designed vertically larger than the pins to avoid transmission of gravity loads through the pins during the tests.

Instrumentation

Instrumentation for this experimental project has been designed to measure global response of the frame, and local performance of beams, columns, and braces, as well as seismic behavior of the BNC isolator installed at the third floor. Global response of the structure in terms of floor accelerations and displacements was obtained from accelerometers and string pots installed at the base of the frame and at every floor. Optical coordinate tracking probes (Krypton sensors) were also distributed on the first story to measure displacement response at specific points.

Seismic response of beams and columns was obtained from strain gauges installed at critical points, to determine whether these members remain elastic during the test, recalling that one of the objectives of this experiment is to assess the effectiveness of the structural fuse concept to prevent damage in beams and columns. Axial deformations of the BRBs were measured with temposonic sensors installed in parallel with the braces and connected to the gusset plates. Temposonic sensors create an electronic pulse interacting with a magnetic field that produces a strain pulse which allows the accurate measurement of axial deformations of the BRBs.

As previously mentioned, a BNC isolator was installed on the third floor of the structure to assess its effectiveness in the protection of nonstructural components. Accelerometers and string pots were installed in three consecutive corners to measure accelerations and displacements in the longitudinal and transverse directions. A detailed description of the instrumentation plan is presented in Vargas and Bruneau (2006b).

Table 2. Bare Frame Maximum Floor Response

Story/PGA (g)	Acceleration (g)				Displacement (mm)				Interstory drift (mm)				Interstory drift (%)			
	0.25	0.50	0.75	1.00	0.25	0.50	0.75	1.00	0.25	0.50	0.75	1.00	0.25	0.50	0.75	1.00
3	0.47	0.94	1.15	1.44	27.15	40.08	57.28	76.48	8.12	15.60	16.47	23.97	0.63	1.21	1.28	1.86
2	0.37	0.65	0.96	1.23	35.27	55.68	73.75	100.45	21.70	36.40	47.24	66.68	1.68	2.82	3.66	5.17
1	0.37	0.73	1.13	1.59	13.57	19.28	26.51	33.77	13.57	19.28	26.51	33.77	1.01	1.44	1.98	2.52

Test Protocol

One of the spectrum compatible synthetic ground motions generated for the parametric study in Vargas and Bruneau (2006a) was used in this experiment as the input ground motion. For similitude purposes, this ground motion was scaled according to the scale factors presented earlier. In the test protocol for the experiment, the amplitude of the ground motion is increased by 0.25 g in each test until the capacity of the shaking table is reached (i.e., which is about 1.0 g for this experiment). Note that a peak ground acceleration (PGA) of 1.0 g is the upper level test value for the experiment. White noise tests (with PGA of 0.10 g) were also performed before and after every earthquake simulation test to identify the dynamic properties of the structure. Two sets of braces were tested following this protocol to examine the replaceability of BRBs as structural fuses.

Experimental Results

Global Response

White noise tests performed after every earthquake simulation test to identify the dynamic properties of the testing frame indicated that the natural frequency of the BF alone (i.e., f_n =1.52 Hz, T_f=0.66 s) was less than for the cases in which additional stiffness is provided by the inclusion of the BRBs (i.e., f_n =3.74 Hz, T_f=0.27 s). Knowing that the stiffness ratio between the BF and BRB frame is inversely proportional to the period ratio to the square [i.e., $K_f/K_1=(T_f/T_1)^2$], it results that the BRB frame was approximately six times stiffer than the BF. This translates into a parameter $\alpha \approx 0.20$, which is in good agreement with the values determined from pushover analyses in the companion paper.

Furthermore, damping ratio was determined using the logarithmic decrement method from the free vibration portion of the motions at the end of every earthquake level simulation. Average damping ratios of 2 and 5% were obtained for the BF and the BRB frame, respectively. The increase in the damping ratio as a function of increases in the magnitude of frame deformations is consistent with what has been observed by others (Vian and Bruneau 2001). Note that the analyses were performed using a damping ratio of 2%, which coincides with the measured values at low amplitude tests, but it is significantly different than the values obtained at higher amplitude tests. This may explain some of the discrepancies observed between experimental and analytical results, as discussed below.

Maximum floor response and interstory drift for the BF and for the BRB frame are presented in Tables 2 and 3, respectively. No significant change was generally observed in the acceleration response between the BF and the BRB frame. The reason for this is that for the actual parameters of this BRB frame the ratio between predicted peak floor acceleration of the structural fuse system with respect to the BF is approximately equal to one (Vargas and Bruneau 2006b). Results in Tables 2 and 3 generally indicate a reduction of approximately 70% in the floor displacement as well as in the interstory drift for the BRB frame with respect to the BF. This significant reduction is an indication of the BRBs effectiveness to control lateral displacements and interstory drifts during strong ground motions (something that is essential to prevent damage to nonstructural components that are attached to consecutive floors). According to the analyses conducted in the companion paper, the anticipated reduction in floor displacement was to be on the order of 77%, which is in reasonably good agreement with the floor demand obtained in the experiment.

Seismic demand in terms of frame ductility, μ_f, and global ductlity, μ, is presented in Table 4. Note that in every story of the BRB frame, the frame ductility is less than one (i.e., $\mu_f < 1$), which is one of the requirements to satisfy the structural fuse concept (recalling that beams and columns remain elastic when the frame ductility is less than one). For the strongest level of earthquake simulation (i.e., PGA=1 g), the average frame and global ductility is 0.7 and 3.4, respectively, which is in good

Table 3. BRB Frame Maximum Floor Response

Story/PGA (g)	Acceleration (g)				Displacement (mm)				Interstory drift (%)			
	0.25	0.50	0.75	1.00	0.25	0.50	0.75	1.00	0.25	0.50	0.75	1.00
(a) Test 1												
3	0.47	0.81	1.10	1.34	5.36	10.06	14.31	18.99	0.21	0.39	0.44	0.65
2	0.32	0.60	0.85	1.10	8.08	15.03	20.02	27.33	0.39	0.78	1.02	1.14
1	0.31	0.69	0.94	0.99	3.07	5.03	6.84	9.18	0.23	0.38	0.51	0.69
(b) Test 2												
3	0.48	0.74	1.02	1.38	5.08	9.48	14.31	21.47	0.17	0.33	0.37	0.49
2	0.30	0.56	0.72	0.96	7.29	13.68	19.14	27.74	0.30	0.64	0.85	1.24
1	0.33	0.68	0.98	1.30	3.38	5.38	8.18	11.78	0.25	0.40	0.61	0.88

Table 4. Ductility Demand

Test/PGA (g)	Frame ductility (μ_f)				Global ductility (μ)			
	0.25	0.50	0.75	1.00	0.25	0.50	0.75	1.00
Bare frame	0.799	1.179	1.685	2.249	0.799[a]	1.179[a]	1.685[a]	2.249[a]
BRB frame 1	0.158	0.296	0.421	0.559	0.766	1.437	2.044	2.713
BRB frame 2	0.149	0.279	0.421	0.631	0.726	1.354	2.044	3.067

[a]Frame and global ductility have the same values for the bare frame.

agreement with the analytical values of 0.62 and 3.10 from charts presented in the companion paper, respectively, for $\alpha \approx 0.20$, $\mu_{max} \approx 5$, $\eta \approx 0.7$, and $T \approx 0.25$ s.

Maximum seismic demand in terms of base shear and roof displacement for every earthquake level is presented in Fig. 6, along with the theoretical pushover curves for the BRB frame and the BF. This figure shows a good correlation between the experimental seismic demand and the analytical pushover curve obtained for the BRB frame.

Local Response

Beam and Column Responses

Bending moments were calculated from strain gauge results at critical locations of beams and columns to assess whether these elements remained elastic throughout the earthquake simulation. From these moments, and using equilibrium equations obtained from a free-body diagram of the columns, it was possible to calculate the shear force at every one of those locations. Then, column shear forces were calculated at every story and results are plotted versus interstory drifts in Fig. 7 for the strongest earthquake level. The elastic behavior exhibited by the frame confirms that the objective of frame protection intended by the structural fuse concept was met. Since the results were experimentally obtained, note that the story shear response is not exactly a straight line (as it was predicted by the analytical model), and some scattering may be observed. However, response points appear to be sufficiently close to the straight line corresponding to the elastic behavior of the frame. In Fig. 6 it may be noted that the shear and interstory drift corresponding to yielding of the BF are 82 kN and 11 mm, respectively (note that in Fig. 7 the shear and drift experimentally obtained for the first story are approximately 50 kN and 4 mm, respectively).

Buckling-Restrained Braces Response

BRBs axial forces were indirectly obtained from the previously calculated internal forces for the beams, as described below. Beam moments and axial forces were determined from strain gauges installed at the ends of the beams. From these moments, and using equilibrium equations obtained from the free body diagrams of the beams, shear forces at the ends of the beams were calculated. Then, BRB axial forces were calculated from equilibrium equations obtained from the free body diagrams including beams and braces.

Table 5 presents a summary of maximum axial deformation of BRBs, at every earthquake level, along with the corresponding ductility. An average ductility of 4.6 can be observed for first and second story BRBs at the strongest level of earthquake. BRBs axial forces and deformations were combined to plot the hysteresis loops presented in Fig. 8. Note that BRBs at first and second

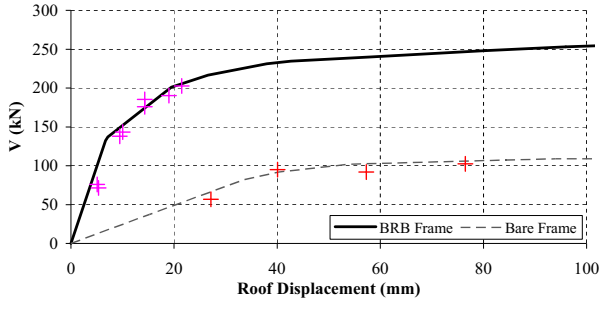

Fig. 6. Seismic demand for bare frame and frame with Nippon steel BRBs

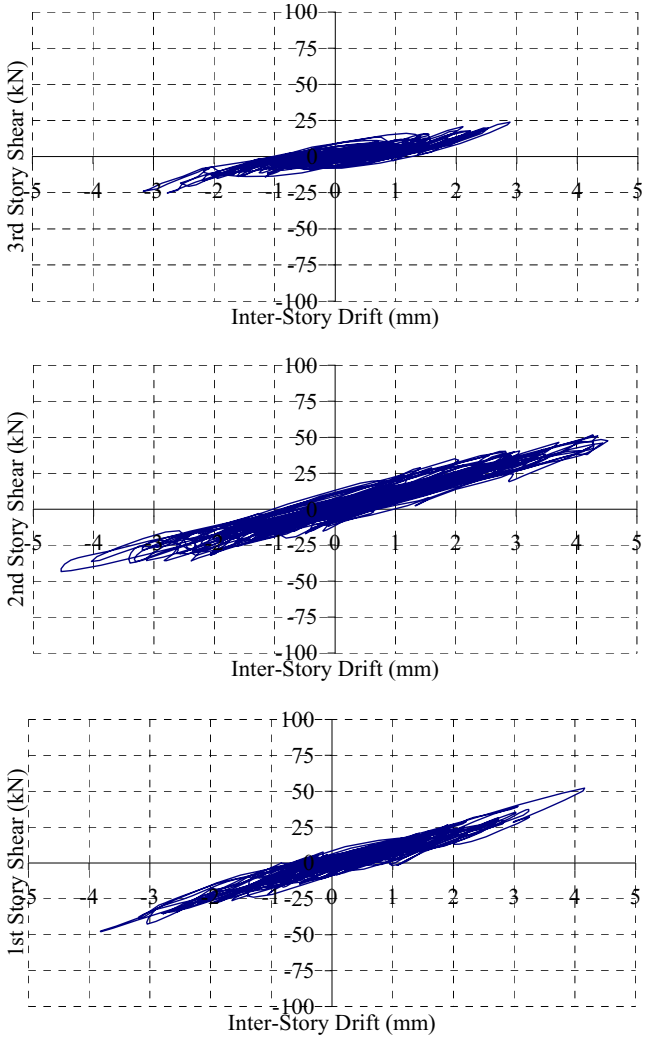

Fig. 7. Columns' story shear for Test 1

Table 5. BRBs Axial Deformation

Story/PGA (g)	Axial deformation (mm)				Ductility (μ)			
	0.25	0.50	0.75	1.00	0.25	0.50	0.75	1.00
(a) Test 1								
3	0.49	0.96	1.06	1.19	0.42	0.82	0.91	1.02
2	0.79	2.62	4.00	5.64	0.68	2.25	3.43	4.84
1	0.84	1.53	3.46	4.98	0.72	1.31	2.97	4.28
(b) Test 2								
3	0.51	0.86	1.12	1.27	0.43	0.74	0.96	1.09
2	0.77	1.87	3.50	5.45	0.66	1.60	3.00	4.67
1	0.87	1.69	3.20	5.40	0.75	1.45	2.74	4.64

stories exhibited inelastic behavior with a ductility of 4.6, while the third story brace remained basically elastic. Note also the apparent increase in the stiffness of the BRB at story one versus the third story brace, which may be attributed to the type of connection used at the base of the frame. Base plates clamped to the shake table were use to connect the frame, and this may have increased the stiffness of the first story with respect to the other two stories.

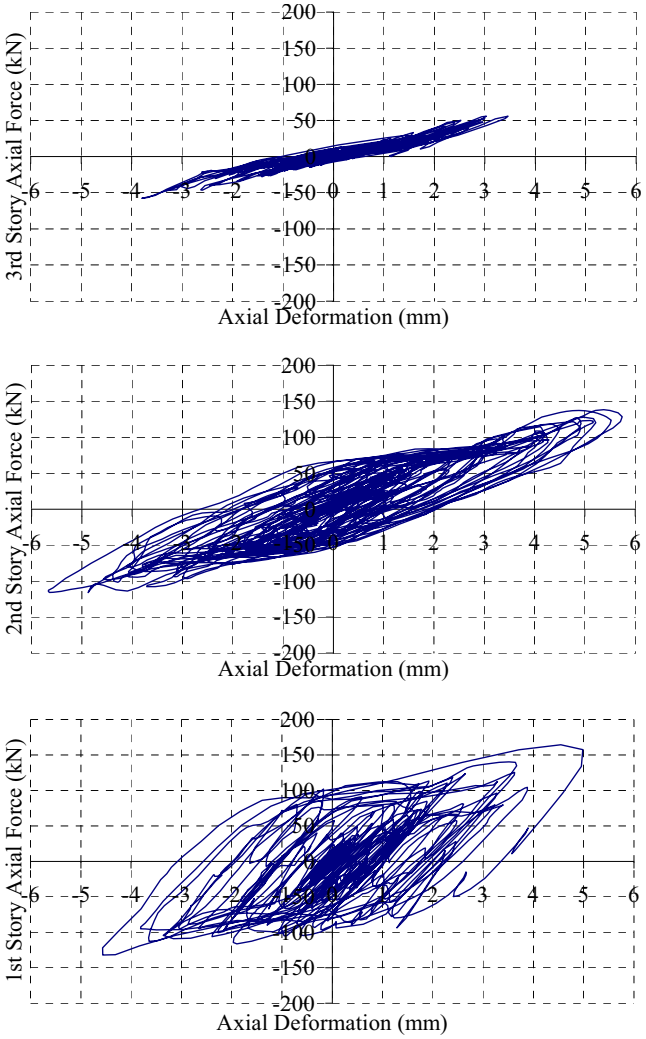

Fig. 8. BRBs hysteresis loops for Test 1

Response of Base Isolator for Nonstructural Components

Seismic response was directly measured from accelerometers and string pots installed on the top platform of the BNC isolator. Acceleration response is presented in Fig. 9, along with the third floor acceleration of the BRB frame (shown as dotted lines). Maximum values of acceleration for both third floor and isolator are presented in Table 6. An almost constant acceleration response can be observed from the results (i.e., 0.14 g on average), regardless of the earthquake level and the structural system (BF or BRB frame). A reduction of 85% in the acceleration response was generally observed from the results, which is in good agreement with the analytical predictions presented in Vargas and Bruneau (2006b).

Isolator response in terms of relative displacement of the top platform with respect to the third floor is also presented in Table 7. Note that when an isolator displacement of 178 mm is reached, the ball travels to the maximum distance to which it can roll. Beyond that, the platform can start to ride on top of the ball and the displacement can increase somewhat beyond that point in an undesirable manner. It may also be noted that for the BRB frames, the isolator did not exceed the maximum allowable displacement, and a general reduction of 50% can be observed with respect to the displacement demand of the isolator installed on the BF. This shows that it is generally possible to reduce the displacement response of BNC isolators compared to BF when additional stiffness is provided by the inclusion of the BRBs (i.e., lateral displacement of the top platform was kept under the limit imposed by the isolator geometry), which may be attributed to the energy dissipation mechanism provided by the BRBs.

Finally, note that the average value of displacement demand for the isolator that would have been used in the corresponding

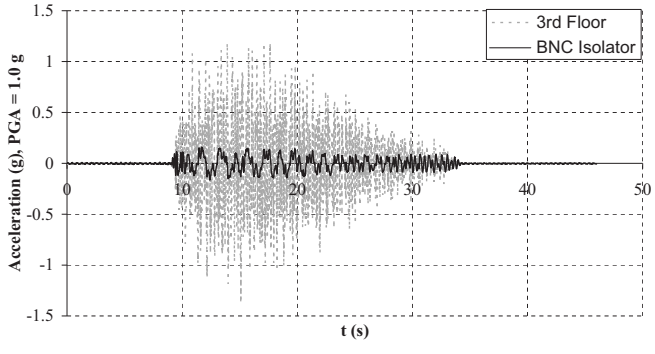

Fig. 9. Acceleration response of isolator for Test 2

Table 6. Acceleration Response of Base Isolator for Nonstructural Components

Test/PGA (g)	Third floor acceleration (g)				Base isolator acceleration (g)				Percent of reduction (%)			
	0.25	0.50	0.75	1.00	0.25	0.50	0.75	1.00	0.25	0.50	0.75	1.00
Bare frame	0.47	0.94	1.15	1.44	0.15	0.17	0.18	0.75	68	82	84	48
BRB frame	0.48	0.74	1.02	1.38	0.12	0.14	0.15	0.16	75	81	85	88

prototype with BRBs, taking all scaling into consideration, would have been 335 mm. Therefore, in actual buildings, such as the prototype used for this study, isolators would generally require such large lateral displacements capacity.

Uniaxial Static Tests

After completion of the shake table tests, the BRBs were axially tested to determine the cyclic performance of the braces based on the acceptance criteria of the seismic provisions for structural steel buildings (AISC 2005) and the Office of Statewide Health Planning and Development (OSHPD). In addition to the standard loading protocol, low-cycle fatigue tests were also conducted until the braces fractured. This was required since these BRBs were the smallest ever manufactured and their ultimate performance had to be ascertained.

Test Setup

The braces were tested on an axial loading facility at the University at Buffalo, which consisted of a foundation beam, reactions blocks, and a hydraulic actuator with a capacity of 222 kN (50 kips). Gusset plates were specifically designed for the BRBs to represent the type of connections used on the shake table tests. One of the gusset plates was attached to a reaction block, the other one was attached to the actuator's head, and the braces were connected to both ends. Fig. 10 shows a schematic view of the setup for the static tests.

Table 7. Displacement Response of Base Isolator for Nonstructural Components

Test/PGA (g)	Base isolator displacement (mm)				Percent of reduction (%)			
	0.25	0.50	0.75	1.00	0.25	0.50	0.75	1.00
Bare frame	67.82	108.95	176.36	204.18	N/A[a]	N/A[a]	N/A[a]	N/A[a]
BRB frame	31.90	48.28	87.40	106.72	53	56	50	48

[a]N/A=not available.

The applied load was measured by a load cell installed in the actuator. According to the seismic provisions for structural steel buildings (AISC 2005) the axial strength of BRBs, P_{ysc}, shall be determined as

$$P_{ysc} = \beta\omega R_y F_{ysc} A_{sc} \tag{7}$$

where β and ω=compression and strain-hardening adjustment factors, respectively; R_y=ratio of the expected yield stress to the specified minimum yield stress; F_{ysc}=specified minimum yield stress of the steel core; and A_{sc}=net area of the steel core. Values of β and ω at the point of maximum deformation were obtained from previous studies (Merritt et al. 2003; Lopez and Sabelli 2004) as 1.2 and 1.6, respectively. R_y was taken as 1.1 from Table I-6-1 from the seismic provisions for structural steel buildings (AISC 2005). Substituting these values into Eq. (7), and recalling that F_{ysc}=235 MPa, and A_{sc}=400 mm^2, values of P_{ysc} were estimated as approximately 200 kN.

Loading Protocol

BRBs were axially tested according to the protocol proposed in the seismic provisions for structural steel buildings (AISC 2005), followed by additional cycles to satisfy the OSHPD requirement for cumulative inelastic deformation.

Table 8 presents the loading sequence for the static tests. Note that the yielding deformation, Δ_{by}, was calculated as 1.17 mm. In this uniaxial brace test series, the brace deformation at the design story drift, Δ_{bm}, was taken as $5\Delta_{by}$ as proposed by seismic provisions for structural steel buildings (AISC 2005).

Once the standard loading protocol was completed for every specimen, low-cycle fatigue tests were conducted with an amplitude of $3\Delta_{bm}$ until the braces fractured. Note that AISC requires the braces to achieve a cumulative inelastic axial deformation of at least $200\Delta_{by}$ before failure. It may be noted from Table 8 that this required cumulative inelastic deformation was exceeded at the end of the standard loading protocol (i.e., $274\Delta_{by}$). In addition, the low-cycle fatigue test conducted until failure amounted to additional cumulative inelastic deformations, and individual results will be reported in the next section.

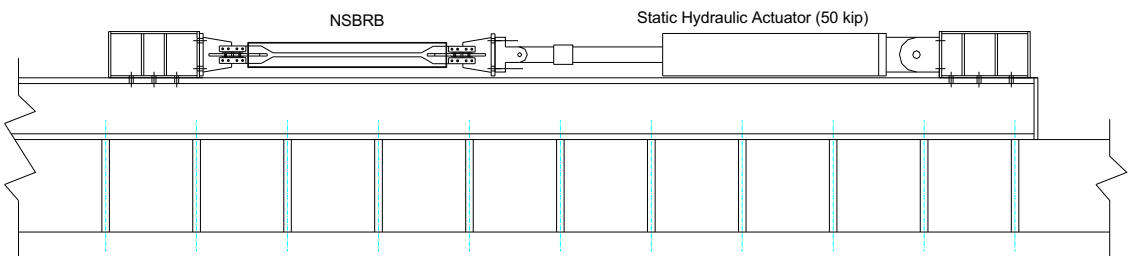

Fig. 10. Static test setup

Table 8. Loading Protocol for Static Test

Cycles	Axial deformation		Inelastic deformation	Cumulative inelastic def.	Axial def. (mm)
4	$0.2\Delta_{bm}$	$1.0\Delta_{by}$	$0\Delta_{by}$	$0\Delta_{by}$	1.17
4	$0.3\Delta_{bm}$	$1.5\Delta_{by}$	$4\Delta_{by}$	$4\Delta_{by}$	1.75
4	$0.5\Delta_{bm}$	$2.5\Delta_{by}$	$12\Delta_{by}$	$16\Delta_{by}$	2.91
4	$1.0\Delta_{bm}$	$5.0\Delta_{by}$	$32\Delta_{by}$	$48\Delta_{by}$	5.83
4	$1.5\Delta_{bm}$	$7.5\Delta_{by}$	$52\Delta_{by}$	$100\Delta_{by}$	8.74
4	$2.0\Delta_{bm}$	$10\ \Delta_{by}$	$72\Delta_{by}$	$172\Delta_{by}$	11.65
2	$2.5\Delta_{bm}$	$12.5\Delta_{by}$	$46\Delta_{by}$	$218\Delta_{by}$	14.56
2	$3.0\Delta_{bm}$	$15\ \Delta_{by}$	$56\Delta_{by}$	$274\Delta_{by}$	17.48

Test Results

Fig. 11 shows the hysteresis loops for the BRBs corresponding to the standard loading protocol and the low-cycle fatigue tests. It may be noted that two types of low-cycle fatigue tests were conducted, with the amplitude of cycles equal to $15\Delta_{by}$ and $20\Delta_{by}$, respectively. Table 9 presents the BRB measured properties along with maximum results. From this table it may be noted that average values of R_y, β, ω, and strain-hardening of 1.15, 1.13, 1.53, and 5%, respectively, matched the target parameters (i.e., $R_y = 1.1$, $\beta = 1.2$, $\omega = 1.6$, and strain-hardening of 4.5%) within 10%. Results obtained at the end of the fatigue life are also shown in Table 9. The maximum cumulative inelastic deformation was $2598\Delta_{by}$, with an average value of $2309\Delta_{by}$, which satisfies the requirement of $200\Delta_{by}$ and translates into a large energy dissipation capacity.

Furthermore, a comparison between the results obtained from static and dynamic tests is presented in Fig. 12 as superimposed curves. Good correlation is observed between static and dynamic test results through the point of maximum displacement achieved during the shake tests.

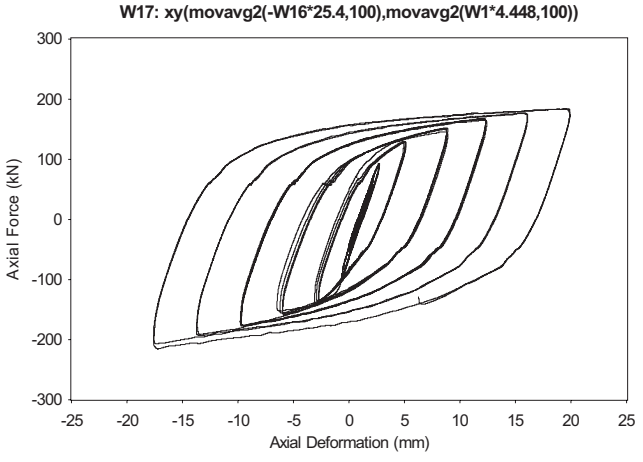

Fig. 11. Hysteretic loops for BRBs static test

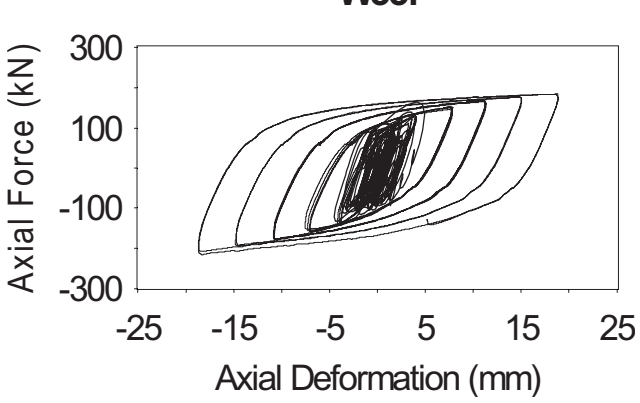

Fig. 12. Comparison between static and dynamic test results

Conclusions

Experimental results presented in this paper indicate that the objectives of the structural fuse concept were successfully achieved (i.e., beams and columns performed elastically, while BRBs worked as metallic fuses and dissipated the seismically induced energy). In general, analytical models reasonably predicted maximum response values for the BRB frame, although some discrepancies were observed in the trend itself. These differences were attributed in part to the fact that the analyses were performed using a damping ratio of 2%, which was found to be lower than the actual values obtained at higher amplitude tests.

Replaceability of BRBs was also found to be feasible by examining this aspect in a test-assessment-replacement-test sequence using four sets of braces connected to the frame by a removable eccentric gusset plate, which were also found to be effective in preventing performance problems observed in other experimental studies with BRBs (e.g., local and out-of-plane buckling of concentrically connected gusset plates). Incidentally, the proposed eccentric gusset-plates detail was found to be effective in preventing performance problems observed in other experimental studies, such as local buckling and out-of-plane buckling of the plates at the connection point. However, since the BRBs were not tested to failure in place in the frame, a final conclusion regarding the performance of that proposed gusset detail should be the subject of further research.

Similarly, BNC isolators were observed to be effective in controlling the acceleration transmitted to nonstructural components in structural fuse systems, where the inclusion of metallic dampers results in a substantial increase in the lateral stiffness. In terms of displacement response, it was observed that it is generally possible to reduce the displacement response of BNC isolators compared to BF by the inclusion of BRBs (i.e., increase in the lateral stiffness of the system).

Table 9. Static Test Results

Test	P_{ysc} (kN)	Δ_{yb} (mm)	K_b (kN/mm)	T_{max} (kN)	C_{max} (kN)	R_y	β	ω	Strain-hard.	Cycles to fract.	Cum. inel. def./Δ_{by}
BRB1	116.09	1.94	59.84	184.31	215.64	1.10	1.17	1.59	0.054	94	2,122
BRB2	123.61	2.09	59.14	203.80	226.90	1.17	1.11	1.65	0.060	97	2,206
BRB3	123.63	2.26	54.70	168.10	187.47	1.17	1.12	1.36	0.043	111	2,598

Acknowledgments

This work was supported in part by the Earthquake Engineering Research Centers Program of the National Science Foundation under Award No. ECC-9701471 to the Multidisciplinary Center for Earthquake Engineering Research. However, any opinions, findings, conclusions, and recommendations presented in this paper are those of the writers and do not necessarily reflect the views of the sponsors.

References

AISC. (2005). "Seismic provisions for structural steel building." *ANSI/AISC 341-05* and *ANSI/AISC 341s1-05*, Chicago.

Amick, H., Bayat, A., and Kemeny, Z. (1998). "Seismic isolation of semiconductor production facilities." *Proc., Seminar on Seismic Design, Retrofit, and Performance of Nonstructural Components, ATC-29-1*, Applied Technology Council, 297–312.

Kasalanati, A., Reinhorn, A., Constantinou, M., and Sanders, D. (1997). "Experimental study of ball-in-cone isolation system." *Building to Last: Proc., 15th Structures Congress*, ASCE, New York, 1191–1195.

Kemeny, Z. A., and Szidarovszky, F. (1995). "Seismic isolation bearings with nonlinear gravity restoring." *Rep. No. MCEER VF01127*, Multidisciplinary Center for Earthquake Engineering Research, State Univ. of New York, Buffalo, N.Y.

Kusumastuti, D., Reinhorn, A., and Rutenberg, A. (2005). "Versatile experimentation model for study of structures near collapse applied to seismic evaluation of irregular structures." *Rep. No. MCEER-05-0002*, Multidisciplinary Center for Earthquake Engineering Research, State Univ. of New York, Buffalo, N.Y.

López, W. A., and Sabelli, R. (2004). "Seismic design of buckling-restrained braced frames." *Steel Tips Rep.*, Structural Steel Educational Council.

Mahin, S. A., Uriz, P., Aiken, I.., Field, C., and Ko, E. (2004). "Seismic performance of buckling restrained brace frame systems." *Proc., 13th World Conf. on Earthquake Engineering*, Vancouver, B.C., Canada, Paper No. 1681.

Merritt, S., Uang, C. M., and Benzoni, G. (2003). "Subassemblage testing of star seismic buckling-restrained braces." *Rep. No. TR-2003/04*, Dept. of Structural Engineering, Univ. of California, San Diego.

Naeim, F., and Kelly, J. (1999). *Design of seismic isolated structures*, Wiley, New York.

Soong, T. T., and Spencer, B. F. (2002). "Supplemental energy dissipation: State-of-the-art and state-of-the-practice." *Eng. Struct.*, 24(3), 243–259.

Tsai, K. C., Hsiao, P. C., Lai, J. W., Weng, Y. T., Lin, M. L., and Chen, C. H. (2004). "International collaboration on pseudo-dynamic tests of a full scale BRB composite frame." *Proc., Workshop of the Asian-Pacific Network of Center in Earthquake Engineering Research* (CD-ROM), Honolulu.

Uriz, P. (2005). "Towards earthquake résistant design of concentrically braced steel buildings." Ph.D. dissertation, Univ. of California, Berkeley, Calif.

Vargas, R., and Bruneau, M. (2006a). "Analytical investigation of the structural fuse concept." *Rep. No. MCEER-06-004*, Multidisciplinary Center for Earthquake Engineering Research, State Univ. of New York, Buffalo, N.Y.

Vargas, R., and Bruneau, M. (2006b). "Experimental investigation of the structural fuse concept." *Rep. No. MCEER-06-005*, Multidisciplinary Center for Earthquake Engineering Research, State Univ. of New York, Buffalo, N.Y.

Vian, D., and Bruneau, M. (2001). "Experimental investigation of P-delta effects to collapse during earthquakes." *Rep. No. MCEER-01-0001*, Multidisciplinary Center for Earthquake Engineering Research, State Univ. of New York, Buffalo, N.Y.